applied sciences

MDPI

Article

A Fluidic Birefringent Sensor for Concentration Measurements of Chemical Solutions in Homodyne Interferometer

Ruey-Ching Twu *, Guan-Min Chen, Jheng-Yu Chen and Nian-Yang Yan

Department of Electro-Optical Engineering, Southern Taiwan University of Science and Technology, Tainan 71005, Taiwan; min790908@gmail.com (G.-M.C.); 499l0016@stust.edu.tw (J.-Y.C.); 4a0l0075@stust.edu.tw (N.-Y.Y.)

* Correspondence: rctwu@stust.edu.tw; Tel.: +886-6253-3131-3628

Academic Editor: Totaro Imasaka

Received: 19 August 2016; Accepted: 20 October 2016; Published: 26 October 2016

Abstract: We have fabricated and tested, to the best of our knowledge, the first fluidic birefringent sensor (FBS) for the concentration measurements of chemical solutions in a homodyne interferometer. The performance of KTP (potassium titanyl phosphate)-based FBS has been experimentally evaluated for successful concentration measurements in salt and hydrochloric acid solutions. The measurement resolution is 0.0088 wt. % in the concentration range of 2.5 wt. % for hydrochloric acid solution. According to the experimental results, the chemical resistance property gives the KTP sensor the potential to be used in harsh environments.

Keywords: optical instruments; birefringent sensors; phase measurement; homodyne interferometer

1. Introduction

Optical birefringence causes two orthogonally polarized propagating lights to have different refractive indices in a birefringent medium. The birefringent materials have been widely used in optical sensors [1–9], polarization holographs [10], waveplates [11] and polarization controllers [12]. Usually, the uniaxial or biaxial crystals with anisotropic properties have polarization-dependent refractive indices. It is possible to make a phase delay between two orthogonal polarizations. It is well known that the reflected light can induce the phase delay of orthogonal polarizations through the principles of surface plasmon resonance (SPR) and total internal reflection (TIR) [13–16]. The variation of phase delay can be measured by utilizing a pair of polarizers according to polarization interferometry. The transmitted birefringent refraction (BR) also can cause the phase delay. Anisotropic materials such as bulk and liquid crystals have been proposed and evaluated for application in optical sensors. In various solid birefringent crystals, the photoelastic, thermo-optic and electro-optic characteristics were adopted for the pressure, temperature and electric field transducers, respectively [1–6]. The birefringent fiber or planar waveguides are also flexible for the compact designs in integrated optic sensors [7,8]. Recently, the liquid crystals have been successfully demonstrated in the application of biosensors due to the birefringence changes induced by the bioreaction [9].

It is essential to monitor liquid concentrations during manufacture and transportation [17,18]. Especially, some chemical solutions are corrosive and a specific metallic sensing head is necessary to monitor the concentrations based on the conductivity dependence response in electronic signals [19]. Since optical probe metrology has remote and non-contact advantages, it can provide a flexible measurement setup. In normal situations, the refractive index (RI) of liquid is concentration-dependent when mixed with different contents. The RI variations of the tested liquids can be detected according to the SPR and TIR sensors in the polarization interferometer [13,16]. Therein, the phase interrogation and

spectra interrogation are less disturbed by the intensity noise of the probe lights. Typically, the optical SPR sensor is fabricated by coating a thin metallic gold film onto a prism or glass sheet. To achieve the highest measurement sensitivity, the thickness and complex RI of the gold film, the incident angle and the probe wavelength have to meet the SPR requirements. Moreover, the tight resonance conditions limit the dynamic range. Although the SPR technique exhibits more sensitivity in comparison with the TIR one, the intrinsic characteristics of the coated metallic layers are easily destroyed in harsh chemical solutions. In a commercial optical instrument for concentration measurements of chemical solutions, the TIR principle utilizing a chemically resistant prism is a typical design for monitoring dynamic concentrations. Since the detected resolution is limited by a beam spot size and a spatial resolution in the CCD camera, it is difficult to improve the concentration resolution down to 0.05 wt. % [20].

The KTP crystal is an important material used for nonlinear optics because of its high resistance to optical damage at short wavelengths. Most of the applications are demonstrated on the wavelength converters [21]. To realize efficient wavelength conversion, a phase-matching condition is achievable under the birefringence effects. For example, it is well known that the green light of 532 nm can be generated by utilizing secondary harmonic generation pumped by a wavelength of 1064 nm. A periodic poling KTP is adopted for various wavelength generations and optical quantum communications [22]. In the previous report [23], the KTP plate has been studied for applications on the concentration measurements of salt liquid by utilizing the BR principle. Because of the KTP's immunity to chemical reactions in some chemical solutions, it can provide possible application in harsh environments. In this study, simulations and experiments have been evaluated to indicate the advantages of the KTP-based birefringence sensor for fluidic liquid concentration measurements. In particular, the varied concentrations of hydrochloric acid (HCL) have been successfully measured with a very low concentration level of 0.0088 wt. %.

2. Measurement Principle and Setup

A schematic of the proposed fluidic birefringent sensor (FBS) is depicted in Figure 1. Its design includes inserting a KTP thin plate in a cylindrical glass cell. When an incident *s*-wave is parallel to the n_z-axis of KTP plate, the phase difference between the two orthogonal *p*- and *s*-waves of the probe light is represented by

$$\phi = \frac{2\pi}{\lambda} \cdot t \cdot \left(\sqrt{n_z^2 - n_i^2 \cdot \sin^2\theta_i} - \sqrt{n_y^2 - n_i^2 \cdot \left(\frac{n_y^2}{n_x^2}\right) \sin^2\theta_i} \right),$$

where γ is the wavelength of the probe light, t is the thickness of the KTP, n_i is the refractive index of the liquid medium and θ_i is the incident angle. The KTP is a biaxial birefringent crystal. There are three different refractive indices represented by n_x, n_y and n_z. The inlet and outlet are connected by a plastic tube. The fluidic liquid is transported by a tubing pump. The phase variation $\Delta\phi$ of the probe beam is dependent on the incident angle and relative refractive index between the KTP plate and the liquid. The liquid's RIs are also dependent on the concentrations of mixed contents. Therefore, the liquid concentrations are measured according to the phase variations.

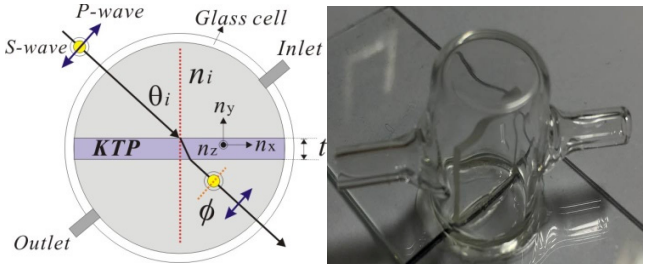

Figure 1. Device structure and photo of a fluidic birefringent sensor (FBS).

Figure 2 represents the schematic diagram of a measurement system for fluidic liquid concentrations. A 632.8 nm He-Ne laser (LS) is used as a probe light in the system. A linear polarizer (PL) and a half-waveplate (HWP) are used to control the probe light with equal power for both orthogonal polarizations. The polarized probe light through an objective lens (L1) is launched into a waveguide-type Zn-indiffused phase modulator (ZIPM) [24]. The sinusoidal voltage from a function generator (FG) is applied on the ZIPM for the homodyne modulations. The output beam is focused through a lens (L2), and a pinhole (PH) is used to filter out the scattering light. The probe beam passes through the FBS, an analyzer (AL), a cylindrical lens (CL) and a photodetector (PD). The tested liquids are injected in the FBS by the tubing pump (TP). The received voltage signals through the PD are connected to a multi-data acquisition module (PXI); the procedure employs a LabVIEW (Version 2010, National Instrument, Austin, TX, USA) platform [24] performed on a personal computer (PC). The measured phase data is saved and shown on the display. In common-path homodyne interferometry, the received interferometric intensity applied with a sinusoidal phase modulation. The modulated interferometric signal is analyzed by a fast Fourier transform (FFT) scheme. The spectrum, with different harmonic signals, can be used for calculating phase information during measurements.

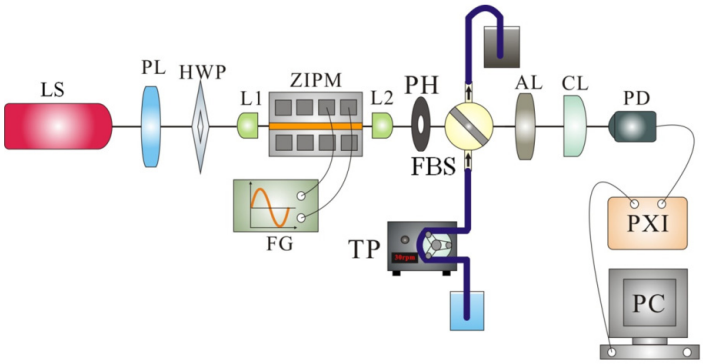

Figure 2. Measurement setup for the fluidic concentration of solution in a homodyne interferometer.

3. Results and Discussions

The simulations of the phase variation $\Delta\phi$ versus RI of the tested liquid medium, ranging from 1.333 to 1.343 refractive index units (RIU) for different incident angles to the surface of the KTP plate (θ_i = 40°~50°), are shown in Figure 3a. The sensitivity of the RI sensor is defined as a slope of the phase curve as shown in Figure 3b. The unit of RI measurement sensitivity is deg./RIU. The sensitivity is increased with the increased incident angle. The linearity is still good for the higher incident angles.

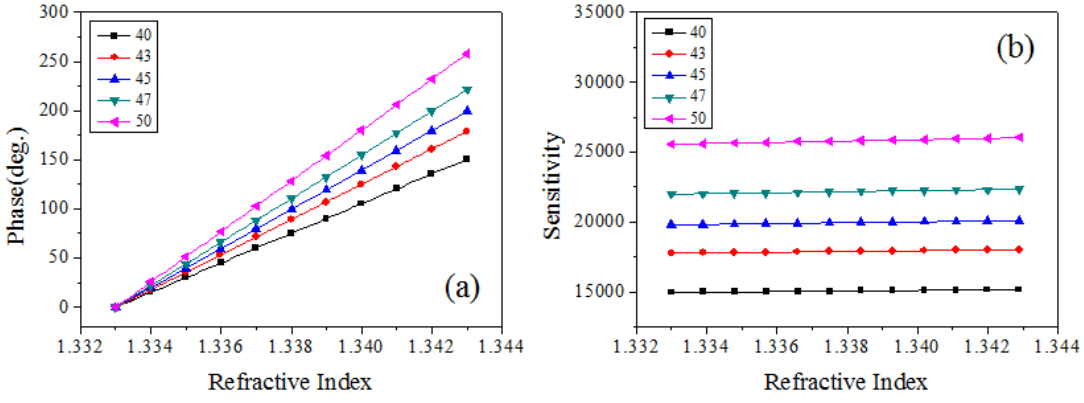

Figure 3. (**a**) Phase change versus RI for different incident angles in a small dynamic range; (**b**) Sensitivity (deg./RIU) versus RI.

Figure 4a shows the phase variation versus RI in a wide dynamic range from 1.30 to 1.50 RIU. The values of sensitivity are dependent on the incident angles and RI regions as shown in Figure 4b. The higher incident angle and larger RI enhance the sensitivity. Because of the relaxed incident angle conditions, its flexibility permits adjustment of the sensitivity for measurements on different levels of concentrations. The sensitivity and linearity on the wide measuring RI range is a tradeoff at the increased incident angle. In a practical application, the nonlinear phase response needs a correction factor to recover the correct measurements.

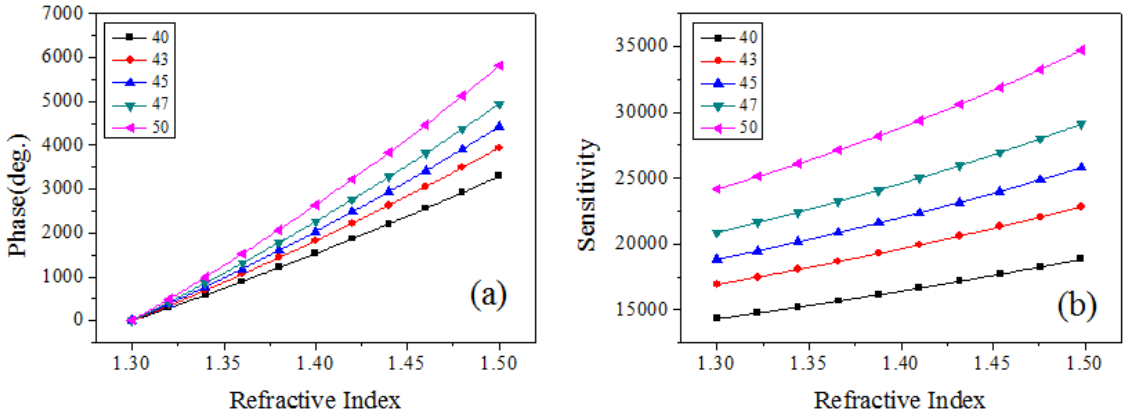

Figure 4. (**a**) Phase change versus RI for different incident angles in a wide dynamic range; (**b**) Sensitivity (deg./RIU) versus RI.

Since the probe beam is focused with a diameter of around 0.2 mm, it is still possible to induce an additional phase shift caused by the photorefractive effects in the KTP plates. At the probe power of 25 μW and a measurement period of 2250 s, the long-term phase variations $\Delta\phi$ in the FBS are within one (degree) with fluidic de-ionized water (DI) at a flow rate of 30 sccm (mL/min), as shown in Figure 5a. The root mean square error (RMSE) of the measured phase data is used to express the phase stability in the measurements. The short-term stability possibly reached 0.2 (degree) during the measurement period of 100 s (200 data points), as shown in Figure 5b. The photo-induced phase variations of the KTP plate will change the initial phase values. It needs a reference injection liquid to obtain the initial phase for providing the reference baseline. The phase variations in the KTP plate are mainly dependent on the wavelengths of incident light and the input powers. The approach to reduce the photorefractive impacts can be considered to reduce the input powers by using a higher-sensitivity photodetector. Besides, the probe light with a longer wavelength (>632.8 nm) is possible to improve the phase stability.

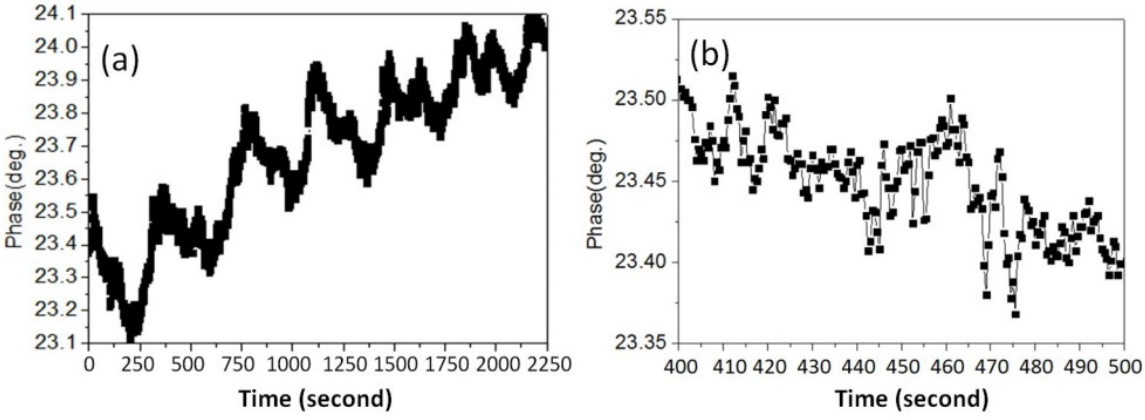

Figure 5. Phase stability measurements: (**a**) long-term period and (**b**) short-term period.

To study the measurement performance depending on the cell sizes, two different designs (Figure 6) are proposed to compare the phase variation profiles under the exchanged liquids between DI and salt water (SW). A quasi-linear dependence of the RI change of the salt solution's concentration (wt. %) is possible [25]. Various RIs can be adjusted by mixing with different weights of water and salt. According to the simulations in Figure 3, the phase variations are expected to have a linear dependence on the concentration. Because of the FBS's cylindrical shape, it is easy to distort the probe beam. The cylindrical lens (CL) is used to focus the transmitted beams onto the PD. There, the large cell has a 28 mm diameter and a height of 16 mm. The small one has a 14 mm diameter and a height of 16 mm. The KTP plates are the same dimensions as used in the two different cells. The length and width of the KTP plate are 8 mm, and the thickness is 1 mm. The KTP plate is placed on the center of cell. The flow rate is 30 sccm (mL/min) from the tubing pump for both cells.

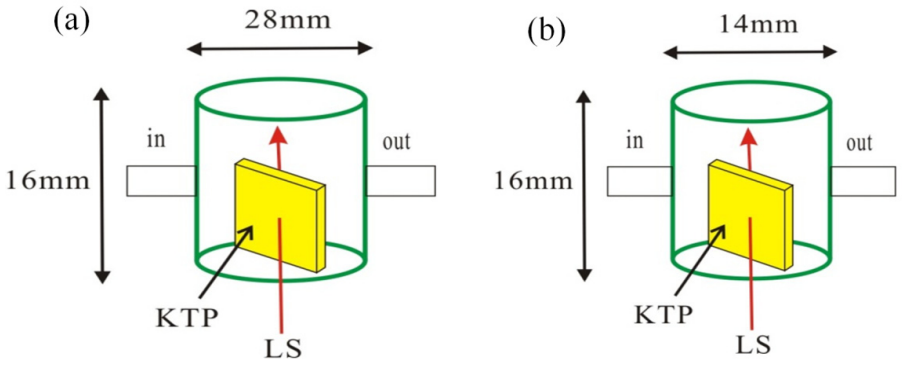

Figure 6. Geometrical sizes of the FBSs: (**a**) large cell and (**b**) small cell.

Figure 7 gives the measurements of phase response for two different incident angles in the large flow cell. The tested concentration of SW is 0.625 wt. %. The values of the phase difference $\Delta\phi$ between DI and SW periods are 25 (degrees) and 35 (degrees) for the incident angles θ_i 45° and 50°, respectively. The trends of phase variation increased as well, as did the incident angle, similar to the simulations shown in Figure 3. The volume of the large cell requires a longer exchange time between the DI and SW liquids; the rise and fall periods also need more time to switch completely. The phase curves of the large cell are rough and include more phase tails during the exchange of liquids.

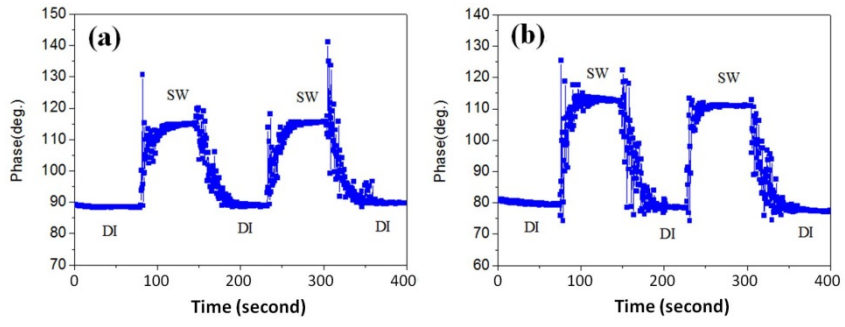

Figure 7. Measurements of phase response for different incident angles in the large flow cell: (**a**) 45° and (**b**) 50°.

To solve these issues, the smaller flow cell (Figure 6b) was adopted for comparing the phase response curves between the two flow cells. At the same flow rate of 30 sccm (mL/min) and the incident angle of 45°, the phase curve of the small cell during the liquid exchanged is shown in Figure 8. The phase difference $\Delta\phi$ between DI and SW is around 24.5 (degrees), which approaches the results of the large cell (Figure 7a). The phase curve is smoother with a near step change. In principle, the phase

variations are possibly increased by increasing the incident angles over 45°. However, the connection ports in the small cell will limit the higher incident angles. To maintain the measurement repeatability, the incident angle of 45° is used for the following experiments.

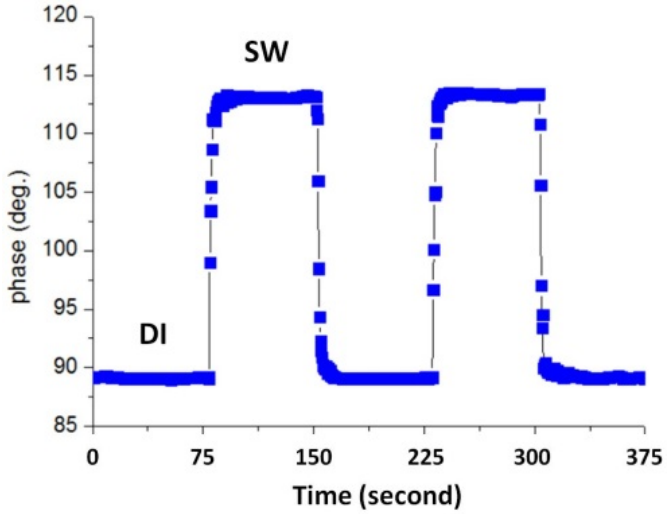

Figure 8. Phase response curve for the small flow cell.

In the optical fluidic instrument, the probe light passes through the liquids in the flow cell. Since the diameters of the inlet and outlet ports are smaller than the cover area of the flow cell. The flow speeds suddenly change between the connection pipe lines and the flow cell will cause turbulent flow [26]. The turbulent flow makes the injection liquids spend more time in the dead volume of flow cell. It will cause the incomplete exchange between two different concentrations of injection liquids. According to the phase curves shown in Figures 7 and 8, the dead-volume effects of the large cell (Figure 7) are obvious in comparison with the small cell (Figure 8).

To calculate the mean values and RMSEs for the different concentrations, the measured phase variations in the central measurement period of 25 s (50 data points) are taken for the SW and HCL solutions. Figure 9a shows the list of the five concentrations of SW: e.g., 0 wt. %, 0.625 wt. %, 1.25 wt. %, 2.5 wt. %, and 5 wt. %. The mean phase change versus the concentration is a quasi-linear curve, as shown in Figure 9b. The summarized table of the mean values and RMSEs is shown in the inset. The phase variation is 135 (degrees) for the 5 wt. % change of concentration. The sensitivity of the concentration measurement is represented by the ratio of the phase difference versus the concentration change. Therefore, the sensitivity is around 2.7×10^3 (deg./wt. %). According to Figure 9c, the liquid switching time is around 15 s to achieve a stable phase change. By considering the stable phase period as shown in Figure 9d, the best phase stability of 0.25 (degrees) is achievable. The corresponding measurement resolution is defined by the ratio of the measurement phase stability versus sensitivity. Thus, the measurement resolution of 0.0092 wt. % is achievable according to the experimental data.

After the optimizations of cell size, focal position and incident angle in the SW concentration measurements, the liquid solution was further replaced by the HCL. Therein, a quasi-linear relationship between the RI and concentration within 40 wt. % was available, as provided in [20]. Figure 10 gives the phase response for different HCLs' concentrations. The periodic modulations of the concentration between the HCL and DI liquids were adopted to test measurement repeatability, as shown in Figure 10a. The mean phase variation versus concentration is shown in Figure 10b. It shows a good linear relation between them. The summarized table of the mean values and RMSEs is shown in the inset. The phase difference is 223 (degrees) in the concentration change range of 2.5 wt. %. Therefore, the sensitivity is around 9×10^3 (deg./wt. %). According to Figure 10c, the liquid switching time is around 9 s to achieve a stable phase change. By considering the stable phase period as shown in Figure 10d, the best phase stability of 0.8 (degree) is achievable in the fluidic HCL solution. Finally, the

measurement resolution of the concentration is 0.0088 wt. %. The chemical stability of the KTP material has been mentioned in [27]. Typically, the chemical solutions used for domain inversion observations of the KTP plate are the mixture of KNO_3 and KOH [28]. The difference of the etching rate between the $+c$ and $-c$ surface of the KTP plate can be used to observe a contrast of the surface morphology. It means that the etching rate is higher on the $-c$ surface (electrical poling) in comparison with the $+c$ surface (without poling). By the way, the chemical etching methods have been widely used to check the defect density after crystal growth. The crystals were put for 60 min into a boiling 37 wt. % HCL solution in order to obtain suitable etch pits [29]. According to the reported etch results [28,29], only the poling regions and defects are easily etched due to the structure changes. Therefore, the idea surface of the KTP plate could be used in harsh environments.

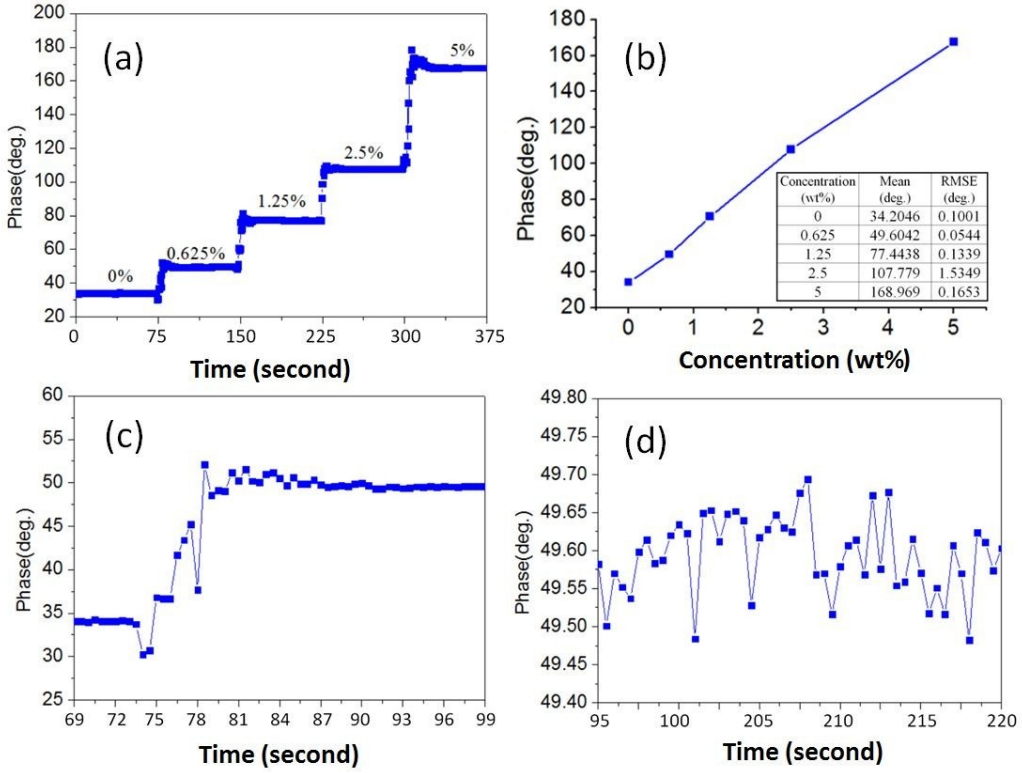

Figure 9. Phase response for different concentrations of SW solution: (**a**) step-increased concentrations of SW; (**b**) phase versus concentration; (**c**) liquid change time; and (**d**) phase stability.

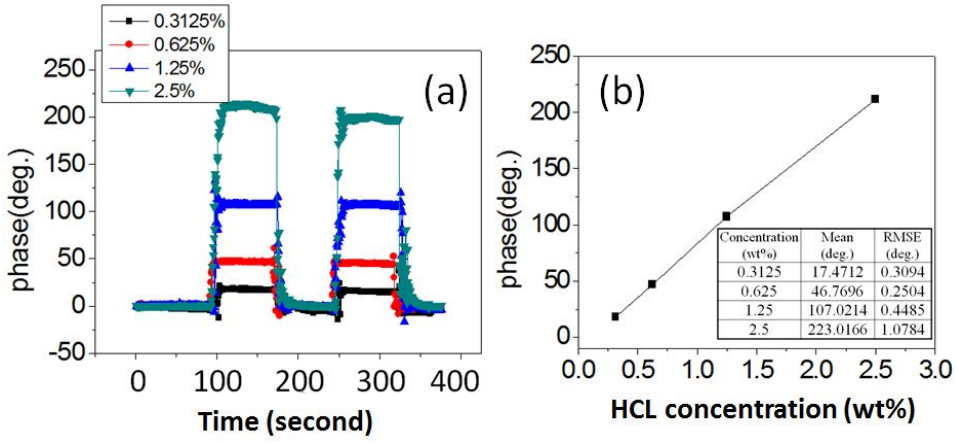

Figure 10. *Cont.*

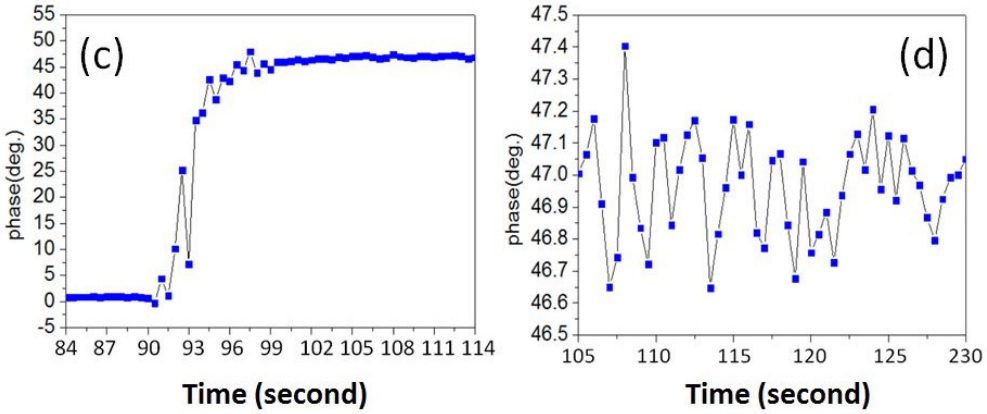

Figure 10. Phase response for different concentrations of HCL solution: (**a**) step exchanged between DI and HCL solutions; (**b**) phase versus concentration; (**c**) liquid change time; and (**d**) phase stability.

4. Conclusions

In summary, the proposed KTP-based FBSs have been successfully demonstrated for the measurements of liquid concentration. The FBSs' designs were systematically evaluated to discuss the measurement performance and optimize the incident angle of the probe light. The repeatable and stable phase measurements were obtained with the simple sensors. The achievable resolutions of concentration were 0.0092 wt. % and 0.0088 wt. % for the SW and HCL solutions, respectively. The RI is around 1.425 RIU for the HCL concentration of 40 wt. % [20]. Although the only low concentration of 2.5 wt. % of HCl solution was used for the first trial experiments, the simulations in Figure 4 offer the possibility that the wide RI (1.30~1.50 RIU) can also be measured in the proposed FBS. Finally, the experimental evidence suggests that with the chemical resistance property, the KTP sensor has the potential for dynamic concentration monitoring of chemical solutions in harsh environments.

Acknowledgments: The authors gratefully acknowledge the financial support provided by Ministry of Science and Technology in Taiwan under grant number MOST 104-2221-E-218-027 for this work.

Author Contributions: Ruey-Ching Twu designed the measurement principles and analyzed the experimental results. Guan-Min Chen, Jheng-Yu Chen, and Nian-Yang Yan conducted the experimental tests and the simulations. Ruey-Ching Twu wrote the paper.

Conflicts of Interest: There are no conflict of interest.

References

1. Li, C. Optical stress sensor based on electro-optic compensation for photoelastic birefringence in a single crystal. *Appl. Opt.* **2011**, *50*, 5315–5320. [CrossRef] [PubMed]
2. Fávero, F.C.; Quintero, S.M.M.; Martelli, C.; Braga, A.M.; Silva, V.V.; Carvalho, I.C.S.; Llerena, R.W.A.; Valente, L.C.G. Hydrostatic pressure sensing with high birefringence photonic crystal fibers. *Sensors* **2010**, *10*, 9698–9711. [CrossRef] [PubMed]
3. Yu, X.; Ma, H.; Jin, Z.; Pan, M.; Hou, L.; Xie, W. Sensitive birefringent temperature sensor based on a waveguide ring resonator. *Appl. Opt.* **2014**, *53*, 2748–2753. [CrossRef] [PubMed]
4. Statkiewicz-Barabach, G.; Carvalho, J.P.; Frazão, O.; Olszewski, J.; Mergo, P.; Santos, J.L.; Urbanczyk, W. Intermodal interferometer for strain and temperature sensing fabricated in birefringent boron doped microstructured fiber. *Appl. Opt.* **2011**, *50*, 3742–3749. [CrossRef] [PubMed]
5. Lee, K.S. Electrooptic voltage sensor: Birefringence effects and compensation methods. *Appl. Opt.* **1990**, *29*, 4453–4461. [CrossRef] [PubMed]
6. Li, C.; Shen, X.; Zeng, R. Optical electric-field sensor based on angular optical bias using single β-BaB2O4 crystal. *Appl. Opt.* **2013**, *52*, 7580–7585. [CrossRef] [PubMed]
7. Sharma, A.K.; Jha, R.; Gupta, B.D. Fiber-optic sensors based on surface plasmon resonance: A comprehensive review. *IEEE Sens. J.* **2007**, *7*, 1118–1129. [CrossRef]

8. Son, G.-S.; Kim, W.-K.; Yang, W.-S.; Lee, H.-M.; Lee, H.-Y.; Lee, S.-D.; Jeong, W.-J.; Kwon, S.-W.; Kim, Y.; Lee, S.-S. Birefringent waveguide sensor using a polarizer rotating technique. *Opt. Lett.* **2009**, *34*, 2045–2047. [CrossRef] [PubMed]
9. Su, H.-W.; Lee, Y.-H.; Lee, M.-J.; Hsu, Y.-C.; Lee, W. Label-free immunodetection of the cancer biomarker CA125 using high-Δn liquid crystals. *J. Biomed. Opt.* **2014**, *19*. [CrossRef] [PubMed]
10. Piron, P.; Blain, P.; Habraken, S.; Mawet, D. Polarization holography for vortex retarders recording. *Appl. Opt.* **2013**, *52*, 7040–7048. [CrossRef] [PubMed]
11. Ishikawa, R.; Kano, R.; Bando, T.; Suematsu, Y.; Ishikawa, S.; Kubo, M.; Narukage, N.; Hara, H.; Tsuneta, S.; Watanabe, H.; et al. Birefringence of magnesium fluoride in the vacuum ultraviolet and application to a half-waveplate. *Appl. Opt.* **2013**, *52*, 8205–8211. [CrossRef] [PubMed]
12. Kim, J.W.; Park, S.H.; Chu, W.S.; Oh, M.C. Integrated-optic polarization controllers incorporating polymer waveguide birefringence modulators. *Opt. Express* **2012**, *20*, 12443–12448. [CrossRef] [PubMed]
13. Homola, J.; Yee, S.S.; Gauglitz, G. Surface plasmon resonance sensors: Review. *Sens. Actuators B Chem.* **1999**, *54*, 3–15. [CrossRef]
14. Zheng, Z.; Wan, Y.; Zhao, X.; Zhu, J. Spectral interferometric measurement of wavelength-dependent phase response for surface plasmon resonance sensors. *Appl. Opt.* **2009**, *48*, 2491–2495. [CrossRef] [PubMed]
15. Watad, I.; Jabalee, M.A.; Aizen, A.; Abdulhalim, I. Critical-angle-based sensor with improved figure of merit using dip detection. *Opt. Lett.* **2015**, *40*, 4092–4094. [CrossRef] [PubMed]
16. Patskovsky, S.; Meunier, M.; Kabashin, A.V. Phase-sensitive silicon-based total internal reflection sensor. *Opt. Express* **2007**, *15*, 12523–12528. [CrossRef] [PubMed]
17. Kashkoush, I.; Rieker, J.; Chen, G. Advanced process control of chemical concentration for solar cell manufacturing. In Proceedings of the 38th IEEE Photovoltaic Specialists Conference (PVSC), Austin, TX, USA, 3–8 June 2012.
18. Yoon, S.; Park, Y.; Cho, K. A new balanced-path heterodyne I/Q-interferometer scheme for low environmental noise, high sensitivity phase measurements for both reflection and transmission geometry. *Opt. Express* **2013**, *21*, 20722–20729. [CrossRef] [PubMed]
19. Rosemount Analytical. Available online: http://www2.emersonprocess.com/en-US/Pages/Home.aspx (accessed on 15 August 2016).
20. Electron Machine Corporation. Available online: http://www.electronmachine.com/pdf/Electron_Chemical.pdf (accessed on 15 August 2016).
21. Jung, C.; Yu, B.-A.; Kim, I.-S.; Lee, Y.L.; Yu, N.E.; Ko, D.-K. A linearly-polarized Nd:YVO4/KTP microchip green laser. *Opt. Express* **2009**, *17*, 19611–19616. [CrossRef] [PubMed]
22. Jin, R.B.; Shimizu, R.; Wakui, K.; Fujiwara, M.; Yamashita, T.; Miki, S.; Terai, H.; Wang, Z.; Sasaki, M. Pulsed Sagnac polarization-entangled photon source with a PPKTP crystal at telecom wavelength. *Opt. Express* **2014**, *22*, 11498–11507. [CrossRef] [PubMed]
23. Twu, R.C.; Chen, G.M. Optical Birefringence sensor for fluidic concentration measurements. In Proceedings of the IEEE Conference on BioPhotonics, Florence, Italy, 20–22 May 2015.
24. Twu, R.C.; Hong, H.Y.; Lee, H.H. Dual-channel optical phase measurement system for improved precision. *Opt. Lett.* **2008**, *33*, 2530–2532. [CrossRef] [PubMed]
25. Lee, J.Y.; Tsai, S.K. Measurement of refractive index variation of liquids by surface plasmon resonance and wavelength-modulated heterodyne interferometry. *Opt. Comm.* **2011**, *284*, 925–929. [CrossRef]
26. Butt, J.B. *Reaction Kinetics and Reactor Design*; Marcel Dekker Inc.: New York, NY, USA, 2000; pp. 332–333.
27. Stolzenberger, R.A. Nonlinear optical properties of flux growth KTiOPO4. *Appl. Opt.* **1988**, *27*, 3883–3886. [CrossRef] [PubMed]
28. Liljestrand, C.; Laurell, F.; Canalias, C. Periodic poling of Rb-doped KTiOPO4 by coercive field engineering. *Opt. Express* **2016**, *24*, 14682–14689. [CrossRef] [PubMed]
29. Bolt, R.J.; van der Mooren, M.; Sebastian, M.T. Etching experiments on flux grown potassium titanyl phosphate KTiOPO4 (KTP). *J. Cryst. Growth* **1991**, *112*, 773–780. [CrossRef]